Bull. Mater. Sci. (2020) 43:275
https://doi.org/10.1007/s12034-020-02248-7

Detailed investigation of the optical properties of the $(C_8H_{11}BrN)_3BiCl_6$ compound by UV–visible measurements

A BEN JAZIA KHARRAT[1,*], KAOUTHER KAHOULI[2] and SLAHEDDINE CHAABOUNI[2]

[1]Laboratoire de Physique des Matériaux, Faculté des Sciences de Sfax, Université de Sfax, BP 1171, 3000 Sfax, Tunisia
[2]Department of Chemistry, Laboratory of Materials Science and Environment, Faculty of Sciences of Sfax, University of Sfax, BP 1171, 3000 Sfax, Tunisia
*Author for correspondence (benjaziaaida@gmail.com)

MS received 16 April 2020; accepted 22 June 2020; published online 9 October 2020

Abstract. The UV–visible studies of the hybrid tris(4-bromo-N,N-dimethylanilinium) hexachlorobismuthate (III) compound [$(C_8H_{11}BrN)_3BiCl_6$], prepared by slow evaporation at room temperature, were investigated in detail from 200–2400 nm. The absorption peaks show the presence of a peak in the UV–C region around $\lambda_{des} = 254$ nm which has the property of disinfecting water. The optical bandgap E_g, determined by both absorbance and reflectance measurements, was estimated to be (3.390 ± 0.009) and (3.354 ± 0.009) eV, respectively. In addition, these measurements approve the direct behaviour of the allowed optical transitions. The low Eurbach energy (128 meV) confirms the high quality of the prepared sample. The dependence on the incident wavelength of the optical constants such as the extinction coefficient k and the refractive index n was discussed. The dispersion parameters E_0 and E_d of this compound were calculated on the basis of the Wemple–Didomenico model. Furthermore, the dielectric studies show that the dissipation factor tan δ has very low value. All the results demonstrate that this compound may be proposed as a good candidate for optical and optoelectronic applications.

Keywords. $(C_8H_{11}BrN)_3BiCl_6$; UV–visible; water disinfection; refractive index; optical bandgap; dielectric conductivity.

1. Introduction

Despite the prohibition of materials having an adverse effect on the environment, the use of polluting materials continues to grow. These compounds which contain heavy metals such as lead, nickel or cadmium, find a multitude of applications in the domestic, medical, industrial, and even agricultural fields. Besides, they can have dangerous effects on health, medical and technological areas and can lead to harmful effects on the environment. In this context, we have focused on hybrid materials. In the last few years, the physical applications of organic–inorganic hybrid compounds, such as ferroelectricity [1–4] and ferroelasticity [5], have become a subject of great interest. These hybrid compounds can constitute a new generation of promising high-performance materials leading to various potential applications due to their particular structure, electric, dielectric and optical properties [6–9]. In addition, these hybrid materials (organic–inorganic) whose preparation is simple and inexpensive, have recently attracted the attention of scientists, leading to their applications in the field of the photovoltaic industry and light absorbers [10,11].

The physical properties of such compounds are strongly related to the properties of both the inorganic anion and the organic cation which can be tuned depending on the required applications [12,13]. An important challenge nowadays, through the use of hybrid materials, is to provide developed electrochemical storage devices such as batteries and super-capacitors which can give important energy values.

The field of this family of materials moving towards its use in the field of optics extends from bio-imaging to optoelectronic devices and even to the design of screens [14]. Indeed, the uniqueness of the optical responses of organic or organometallic molecular species lead to the development of innovative hybrid compounds, on a macro or even nanometric scale.

In this context, a new organic–inorganic metal halide (OIMHs) tris(4-bromo-N,N-dimethylanilinium) hexachlorobismuthate (III) $(C_8H_{11}BrN)_3BiCl_6$ has been synthesized by slow evaporation at room temperature. This sample is characterized by the existence of spaces between the inorganic entities which are filled by organic cations through hydrogen bonds in order to provide their connection.

The crystal lattice of this compound is built up from the packing of distorted $[BiCl_6]^{3-}$ octahedra surrounded by $[C_8H_{11}BrN]^+$ organic cations. The cohesion of the structure is achieved by an extensive network of N–H···Cl and

C–H···Cl hydrogen bonds. In the previous study [15], the Hirshfeld surface analysis associated with 2D fingerprint plots were used to visualize and explore the significant intermolecular interactions in the crystal structure quantitatively. The infrared and Raman spectra were recorded in the 4000–400 and 4000–50 cm^{-1} frequency regions, respectively, and they were compared with those found in homologous compounds in the literature. The ^{13}C CP-MAS NMR spectrum is in full agreement with the crystallographic data determined by X-ray structure. At ambient temperature, optical absorption UV–visible and photoluminescence (PL) spectra of this material were interpreted and analysed by comparison with those of the homologous hybrids.

Particularly, PL and optical absorption measurements carried out at ambient temperature reveal the presence of a strong emission in the violet range of energy located at 2.92 eV (424 nm).

It is clear that the investigation of the UV–visible optical absorption, reported in ref. [15] seems to be incomplete and insufficient to give all optical characteristics of the proposed hybrid material which can be used for optical applications.

The main aim of this study is to investigate in detail the optical properties of the $[(C_8H_{11}BrN)_3BiCl_6]$ hybrid compound through UV–visible measurements performed at room temperature. The determination of the optical parameters is decisive for the choice of a compound which may be used on the basis of an optoelectronic device.

2. Experimental

As reported in the previous study [15], the single crystal $(C_8H_{11}BrN)_3BiCl_6$ sample was successfully prepared by slow evaporation at room temperature. The obtained compound was dried and prepared in order to perform optical measurements. The X-ray diffraction investigation reveals that the compound crystallizes in the orthorhombic system with the non-centrosymmetric space group $P2_12_12_1$. The obtained unit cell parameters are: a = 9.2820(3) Å, b = 13.7960(5) Å, c = 27.4298(12) Å, V = 3512.5(2) $Å^3$ with Z = 4. The asymmetric unit of this sample is formed by the monomeric $[BiCl_6]_3$ anion and three protonated 4-bromo-N,N-dimethylanilinium cations.

The UV–visible measurements were obtained, at room temperature, by a UV-3101PC scanning spectrophotometer using a source emitting wavelength radiations which varies from 200–2400 nm.

3. Results and discussion

3.1 *Determination of the optical bandgap E_g*

The objective of studying the optical measurements is to determine the principal properties of this compound such as the optical energy bandgap, the Urbach energy, the extinction coefficient, the refractive coefficient as well as the optical conductivity in order to select its appropriate area of application.

Figure 1 portrays the room temperature UV–visible absorption spectrum $A(\lambda)$ of the synthesized $(C_8H_{11}BrN)_3BiCl_6$ compound as a function of the incident wavelength λ. As shown, the absorption edges were found to be in the ultraviolet region, which means that the sample can be used in photovoltaic applications or light photocatalysis. The detected strong absorption in this region can be associated with the electronic transition from the valence band to the conduction band.

A first brief optical study of this compound shows that it exhibited two dominant bands located at 254 and 322 nm. Indeed, the first one around 254 nm is associated with the transitions of type $\pi \rightarrow \pi^*$ characteristic of the organic $[C_8H_{11}BrN]^+$ cations and the second one located at 322 nm can be assigned to Ligand to Metal Charge Transfer (LMCT) transition. A deeper investigation of the first absorption peak shows that this peak is located in the UV–C region ($200 \leq \lambda \leq 280$ nm) at λ_{des} = 254 nm. This particular

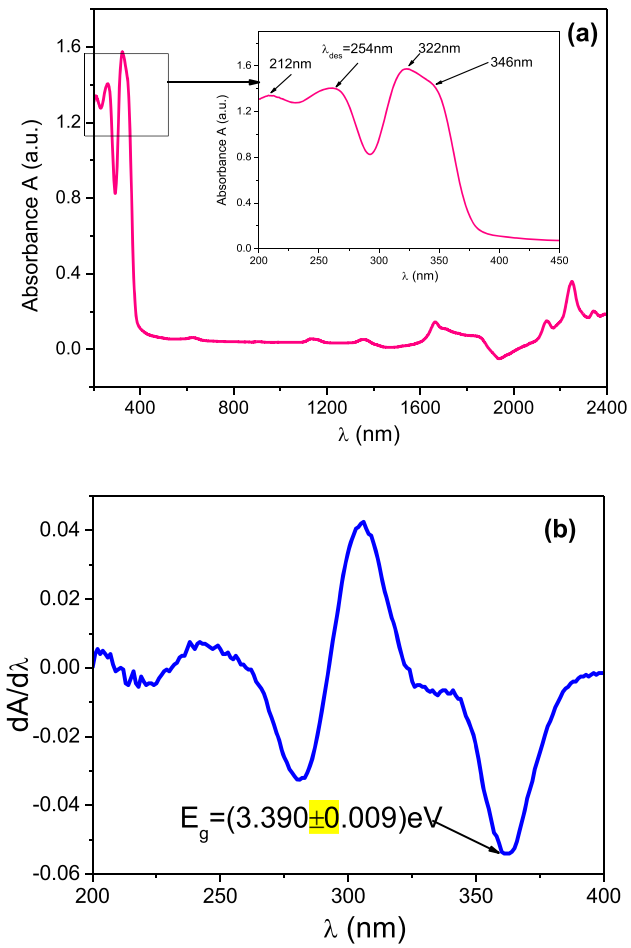

Figure 1. (**a**) Evolution of the absorption coefficient A of the $(C_8H_{11}BrN)_3BiCl_6$ sample as a function of wavelength and (**b**) the variation of $dA/d\lambda$ with λ for the $(C_8H_{11}BrN)_3BiCl_6$ compound.

wavelength has the property of disinfecting water using the long ultraviolet radiation 254 nm wave. Indeed, the UV–C rays inactivates and/or destroys the DNA of bacteria and viruses harmless to human health. In addition, with this chemical disinfection method, not all micro-organisms react in the same way when exposed to radiation which gives the possibility of exploiting this compound in this application in the UV–C region. It should also be noted that some micro-organisms are made inactive with a relatively small amount of UV rays, but others need larger doses to get the desired activation percentages. It is worth noticing that the peak observed at 322 nm was assigned to the LMCTT from the $np(t_{1g}t_{2g}t_{1u}t_{2u})$ orbital of Cl to $6p(t_{1u})$ orbital of Bi^{3+}, whereas the peak located at 262 nm (in the vicinity of λ_{des}) is correlated with the 6s6p metal centred transition from the $6s^2$ to the T_{1u} state which is related to the $^3P1$ atomic state in Bi^{3+} [15].

The inset of figure 1 shows the variation of $dA/d\lambda$ with λ. The optical bandgap E_g of this studied compound can be determined from the minimum of the $dA/d\lambda$ curve in the high energy side. The obtained value is (3.390 ± 0.009) eV characterizing $(C_8H_{11}BrN)_3BiCl_6$ as a wide bandgap material. This method does not make it possible to distinguish whether the gap is direct or indirect. For this, we used the Tauc's method based on the following relation [16]:

$$A{\cdot}h\nu = B\left(h\nu - E_g\right)^n, \tag{1}$$

where $h\nu$ is the energy of the incident photon, B is a parameter characterizing the degree of disorder which may occur in the studied compound and the value of n provides information on the nature of the transition: n = 0.5 for an allowed direct transition and n = 2 for an allowed indirect bandgap [17]. The plot of $(Ah\nu)^{0.5}$ and $(Ah\nu)^2$ *vs.* $h\nu$ is shown in figure 2. The bandgap E_g (E_{gd} and E_{gi} are respectively the direct and the indirect bandgap) can be evaluated through the extrapolation of the linear part of each curve [18]. The bandgap is estimated to be (3.351 ± 0.168) eV for n = 0.5 and (4.150 ± 0.151) eV for n = 2.

In order to verify the n value, we have plotted in figure 3 the evolution of $\mathrm{Ln}(Ah\nu)$ against $\mathrm{Ln}(h\nu - E_g)$ used as trial values for E_g, those obtained previously according to the expression:

$$\mathrm{Ln}(Ah\nu) = \mathrm{Ln}\ B + n\,\mathrm{Ln}\left(h\nu - E_g\right). \tag{2}$$

The fit of the linear part of each curve gives n = 0.505 for E_{gd} = 4.150 eV and n = 0.551 for E_{gi} = 3.351 eV confirming the direct bandgap of the studied compound. This value (3.351 eV) is higher than those obtained for other hybrid materials. Indeed, the optical bandgap E_g is evaluated at 3.11, 3.04 and 2.4 eV for $(C_2H_5NH_3)_2CdCl_4$, $(C_2H_5NH_3)_2Cd_{0.5}Cu_{0.5}Cl_4$ and $(C_2H_5NH_3)_2CuCl_4$ compounds, respectively [19]. On the other hand, some hybrid compounds show high bandgap values such as $[(CH_3)_2NH_2]_2ZnCl_4$ (E_g = 4.26 eV) [20].

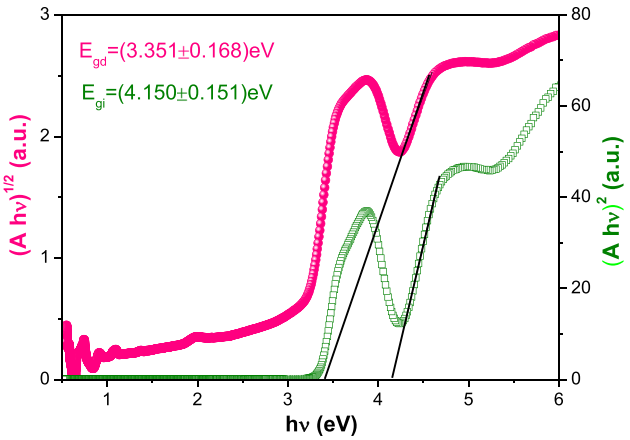

Figure 2. Plot of $(Ah\nu)^{1/2}$ and $(Ah\nu)^2$ against $h\nu$ (E_{gd} and E_{gi} are respectively the direct and the indirect bandgap) for the $(C_8H_{11}BrN)_3BiCl_6$ compound.

Figure 4 displays the evolution of the reflectance R relative to the $(C_8H_{11}BrN)_3BiCl_6$ compound against wavelength. As illustrated, this material shows importance of reflectance in the visible and IR domains. This selective property confirms that the studied compound may be used in applications in the ultraviolet domain. In the inset of figure 4a, we have plotted the variation of $dR/d\lambda$ *vs.* λ. The optical bandgap E_g relative to this compound determined from the maximum of the $dR/d\lambda$ curve in the high-energy side [21] is (3.354 ± 0.009) eV. We can notice that this method proposed by Marotti *et al* [22] confirms the direct bandgap of the studied compound.

3.2 *Determination of the Urbach energy E_u*

For the purpose of the determination of the pre-absorption edge, we have determined the Urbach tail E_u characterizing disordered and amorphous materials. Indeed, E_u, which depends weakly on temperature, is often interpreted as the width of the tail relative to localized states located between valence and conduction bands. According to Urbach model [23], E_u can be calculated using the following expression where C is a constant:

$$A = C\exp\left(\frac{h\nu - E_g}{E_u}\right). \tag{3}$$

Using this exponential relation, the Urbach energy E_u can be easily determined from the slope of $\mathrm{Ln}(A)$ as a function of energy $h\nu$ shown in figure 5a. The calculated value of E_u is (128 ± 2) meV, proves the presence of a small disorder in this hybrid compound. In addition, E_u represents only 3.7% of the bandgap value confirming the good quality of this compound.

On the other hand, the Urbach energy (E_u) can be related to the steepness parameter S by the expression [24]:

$$E_u = k_B T/S(T). \tag{4}$$

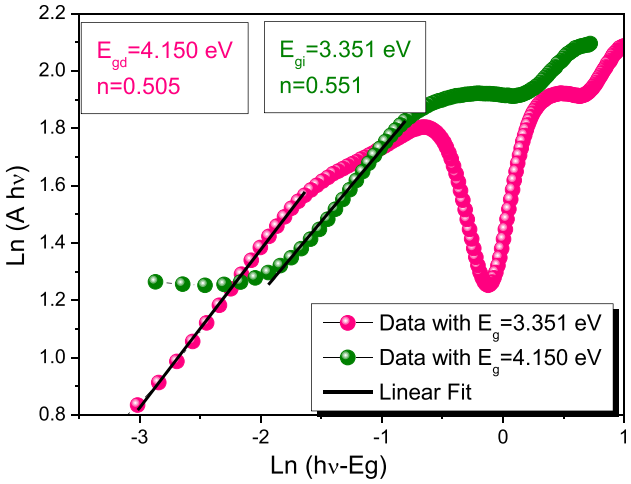

Figure 3. Evolution of Ln(Ahv) *vs.* Ln(hv – E_g) for the $(C_8H_{11}BrN)_3BiCl_6$ compound.

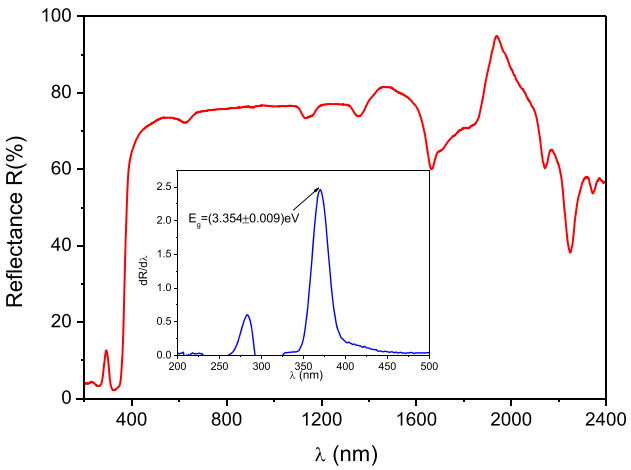

Figure 4. Evolution of the reflectance R of the $(C_8H_{11}BrN)_3BiCl_6$ compound as a function of wavelength. The inset shows the variation of dR/dλ with λ.

The calculated value of the steepness parameter is 202 × 10^{-3}.

Another parameter used to evaluate the importance of this compound in optoelectronic devices is the maximum wavelength λ_T, of incident radiation, currently defined as threshold wavelength, which is required to eject charge carriers. The value of λ_T can be determined using the following expression [25,26]:

$$\left(\frac{A}{\lambda}\right)^2 = D\left(\frac{1}{\lambda} - \frac{1}{\lambda_T}\right). \quad (5)$$

In this relation, D is a constant. So, we have plotted the $(A/\lambda)^2$ curve *vs.* $1/\lambda$ to find out the threshold wavelength λ_T as shown in figure 5b. The obtained value of λ_T = 402 nm.

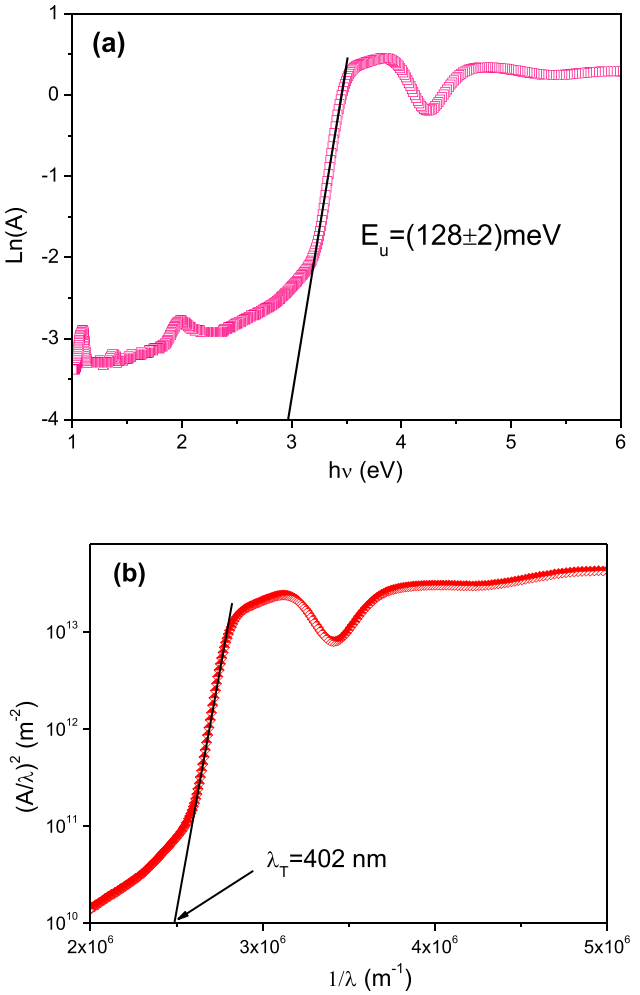

Figure 5. (**a**) Ln(A) *vs.* hv plots to determine the Urbach energy E_u and (**b**) $(A/\lambda)^2$ *vs.* $1/\lambda$ plots for the $(C_8H_{11}BrN)_3BiCl_6$ compound.

3.3 *The penetration depth and optical extinction*

The penetration depth δ is defined as the measure of how electromagnetic radiation or a deep light can penetrate into a compound. Theoretically, from an intensity point of view, δ is the depth at which the incident intensity of the radiation falls to 1/e as compared to its original value. Using the absorption data, the penetration depth (or skin depth) can be evaluated using the expression [24]:

$$\delta(\lambda) = 1/A(\lambda). \quad (6)$$

Figure 6 portrays the evolution of the penetration depth δ against radiation wavelength relative to the $(C_8H_{11}BrN)_3BiCl_6$ material. As illustrated, the curve of $\delta(\lambda)$ shows three regions. In region I, this sample acts as a screen effect for wavelengths $200 \leq \lambda \leq 365$ nm. Such a result is important since this sample can eliminate ultraviolet radiation. In region II, a small penetration may be observed and it is almost constant for $365 \leq \lambda \leq 1355$ nm. In region III, a

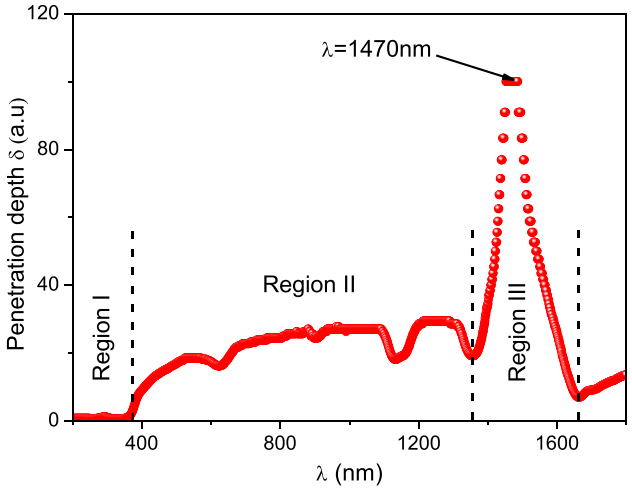

Figure 6. Variation of the penetration depth δ against λ for the studied $(C_8H_{11}BrN)_3BiCl_6$ material.

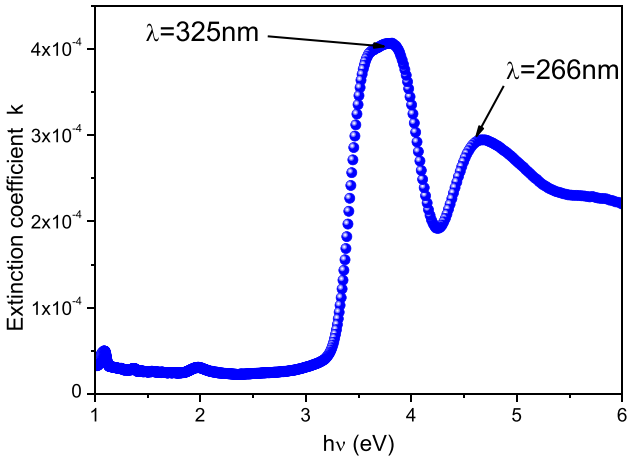

Figure 7. Evolution of the optical extinction k *vs.* $h\nu$ for the $(C_8H_{11}BrN)_3BiCl_6$ compound.

particular peak was observed for λ = 1470 nm which belongs to the domain of X-rays.

Furthermore, the optical extinction k *vs.* wavelength λ can be calculated using the expression [27]:

$$k(\lambda) = \frac{A(\lambda)\lambda}{4\pi}. \tag{7}$$

Figure 7 displays the variation of the optical extinction k as a function of λ for this prepared sample. As clearly shown, the k curve shows two particular maximums located in the UV domain at 266 and 325 nm.

3.4 *The refractive index of the $(C_8H_{11}BrN)_3BiCl_6$ compound*

In the visible domain, the optical refractive index n can be calculated by using the following expression [28]:

$$n(\lambda) = \frac{1+R}{1-R} - \sqrt{\frac{4R}{(1-R)^2} - k^2}. \tag{8}$$

Figure 8a displays the evolution of the optical refractive index as a function of the wavelength λ at room temperature for the $(C_8H_{11}BrN)_3BiCl_6$ compound. As illustrated, n depends strongly on the wavelength. The n curve shows the highest value in the UV region, then it decreases with an increase in the wavelength. Beyond 400 nm, the value of n is around 1.5. Such remarkable transparency may be attributed to low scattering and absorption losses. A deeper examination of the evolution of n in the visible spectrum is presented in figure 8b.

The refractive index n can be expressed as a function of the wavelength λ using the well-known Cauchy's relation given by:

$$n = n_0 + \frac{n_1}{\lambda^2} + \frac{n_2}{\lambda^4}. \tag{9}$$

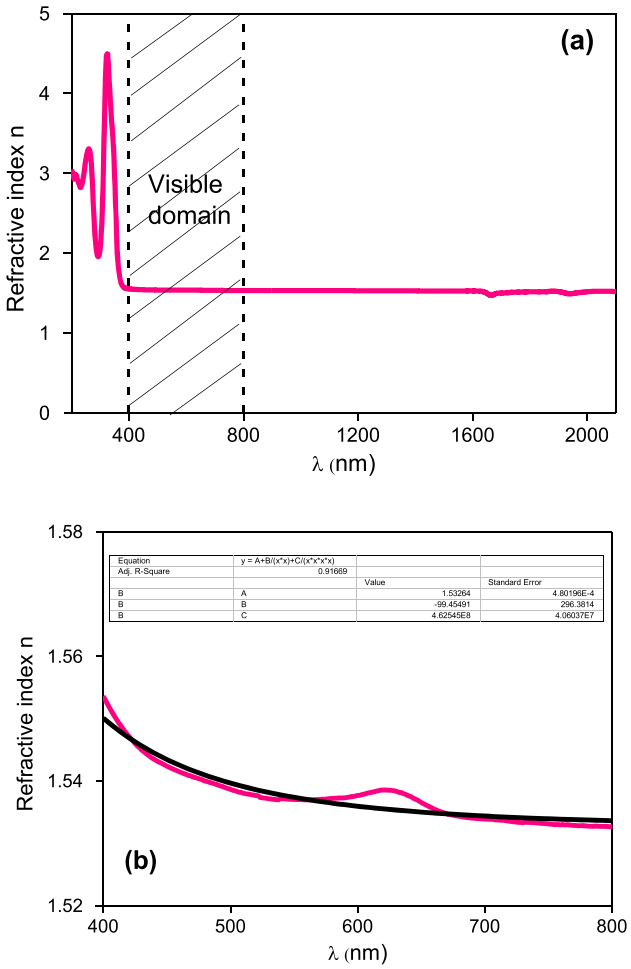

Figure 8. (**a**) Evolution of the refractive index n as a function of incident photon wavelength λ and (**b**) Fit of n using the Cauchy's relation in the visible domain for the $(C_8H_{11}BrN)_3BiCl_6$ compound.

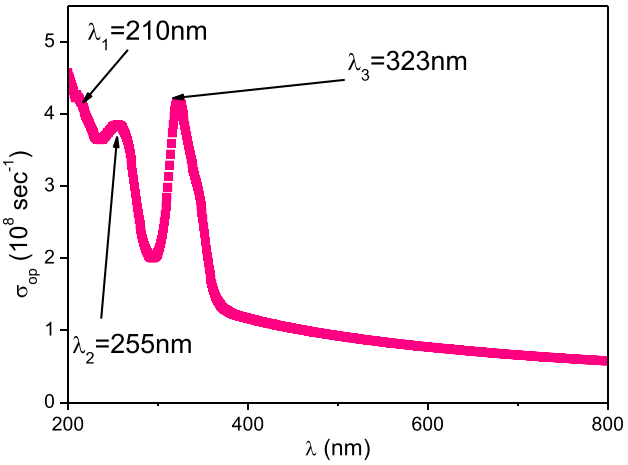

Figure 9. Evolution of the optical conductivity σ_{op} against the incident photon wavelength λ for the $(C_8H_{11}BrN)_3BiCl_6$ compound.

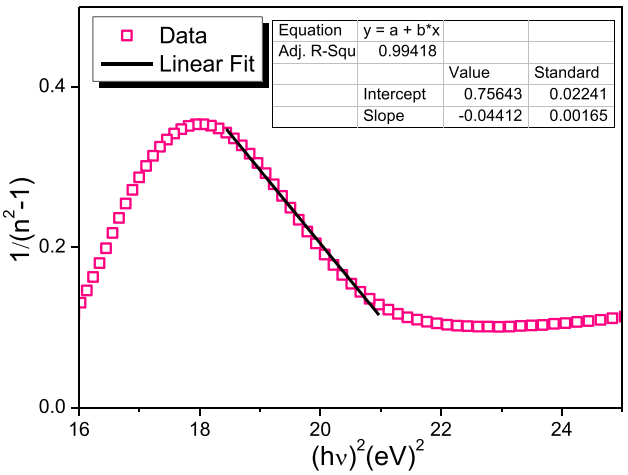

Figure 10. Plot of $1/(n^2 - 1)$ against the incident energy $h\nu$ for the $(C_8H_{11}BrN)_3BiCl_6$ compound.

The fit of our experimental data with relation (9), illustrated in figure 8b, gives the values of the Cauchy's constants: $n_0 = 1.533$, $n_1 = -99.455$ $(nm)^2$ and $n_2 = 4.625\times10^8$ $(nm)^4$.

3.5 *Evolution of the optical conductivity and dispersion energy parameters*

Theoretically, the optical conductivity σ_{op} depends on optical parameters such as the absorption coefficient A, the refractive index n and the extinction coefficient k. This parameter can be calculated by using the following relation [24]:

$$\sigma_{op}(\lambda) = \frac{A(\lambda)n(\lambda)c}{4\pi k(\lambda)}, \tag{10}$$

where c denotes the speed of light in free space (or air).

The evolution of the optical conductivity σ_{op} with wavelength for the $(C_8H_{11}BrN)_3BiCl_6$ compound is illustrated in figure 9. As illustrated, three peaks corresponding to a maximum of conductivity can be detected at $\lambda_1 = 210$, $\lambda_2 = 254$ and $\lambda_3 = 323$ nm located in the UV domain. This result shows that the incident photon energy induces more excited electrons at these selective wavelengths, in particular $\lambda_2 = \lambda_{des}$ which can be used for disinfecting water as proposed previously. In addition, this compound can be used as an optical filter in the UV region.

The energy of the effective single oscillator E_0 and the dispersion energy E_d characterizing the intensity of the inter-band optical transitions can be computed through the relation proposed by Wemple–Didomenico [29]:

$$n^2 - 1 = \frac{E_0E_d}{E_0^2 - (h\nu)^2}. \tag{11}$$

Thus, the E_0 and E_d values can be determined by fitting the linear part of the $1/(n^2 - 1)$ curve *vs.* $(h\nu)^2$ as seen in figure 10. The slope of this curve gives $1/(E_0E_d)$ and its intercept with the vertical axis gives E_0/E_d. The obtained values are $E_0 = 4.715$ eV and $E_d = 6.233$ eV. We can remark particularly that $E_0 = 1.39E_g$ ($E_g = 3.390$ eV). This result agrees approximately with the relation $E_0 = 1.376E_g$ obtained using the single oscillator model [30].

The E_0 and E_d values can be used to evaluate the zero frequency dielectric constant ε_{op} and the static refractive index n' defined for $(h\nu)^2 = 0$ in relation (11) by:

$$\varepsilon_{op} = 1 + \frac{E_d}{E_0} = n'^2. \tag{12}$$

The obtained values of ε_{op} and n' are 2.322 and 1.524, respectively. The value of n' is close to that obtained from the fit by Cauchy's law.

On the basis of the same model, we have also evaluated the oscillator wavelength λ_0 and the average oscillator strength S_0 relative to the $(C_8H_{11}BrN)_3BiCl_6$ compound using the following relation [31]:

$$\frac{1}{n^2 - 1} = \frac{1}{S_0\lambda_0^2} - \frac{1}{S_0\lambda^2}. \tag{13}$$

We have reported in figure 11 the plot of $(n^2 - 1)^{-1}$ *vs.* $(\lambda)^{-2}$. From the linear fitting, we have noticed that the obtained values ($S_0 = 7.454\times10^{-13}$ m^{-2} and $\lambda_0 = 262.5$ nm) are in the same order of those obtained from other compounds such as $[(CH_3)_3NH]CdCl_3$ [32], $Cd_{50}S_{50-x}Se_x$ [33] and $Ge_{20}Se_{60}Sb_{20-x}Ag_x$ (x = 0, 5, 10, 15 and 20 at%) [34].

On the other hand, we have calculated the moments of the optical spectrum M_{-1} and M_{-3}, which determine the average bond strength from the relations [34]:

$$E_0^2 = \frac{M_{-1}}{M_{-3}} \quad \text{and} \quad E_d^2 = \frac{M_{-1}^3}{M_{-3}}. \tag{14}$$

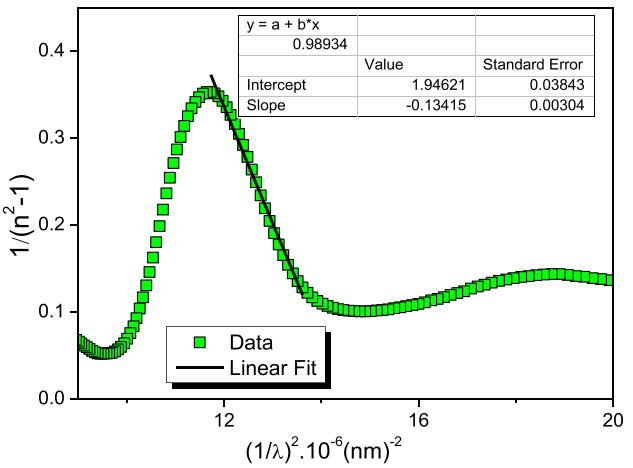

Figure 11. Plot of $1/(n^2 - 1)$ *vs.* $(1/\lambda)^2$ for the $(C_8H_{11}BrN)_3BiCl_6$ compound.

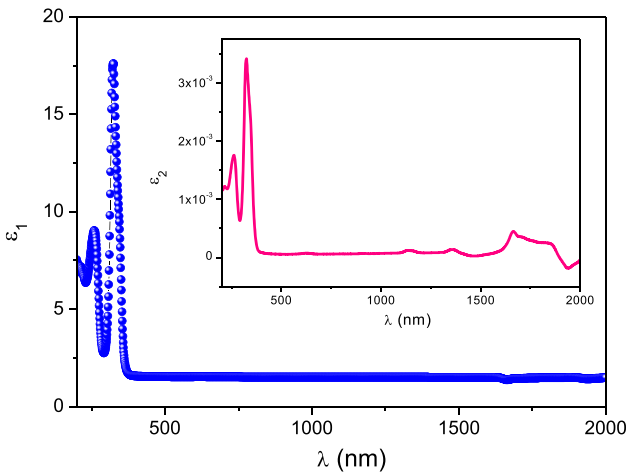

Figure 12. The plots of the real part ε_1 and the imaginary part ε_2 (in the inset) of the dielectric permittivity *vs.* λ for the $(C_8H_{11}BrN)_3BiCl_6$ compound.

The obtained values are $M_{-1} = 1.322$ and $M_{-3} = 0.059$ $(eV)^{-2}$.

3.6 *Dielectric studies*

The real and imaginary parts of the complex dielectric constant $\varepsilon^*(\lambda)$ relative to the $(C_8H_{11}BrN)_3BiCl_6$ compound were computed using the refractive index $n(\lambda)$ and the extinction coefficient $k(\lambda)$ based on the following relation [35]:

$$\varepsilon^*(\lambda) = \varepsilon_1(\lambda) - i\varepsilon_2(\lambda) = [n(\lambda) - ik(\lambda)]^2. \quad (15)$$

Thus, the real part (ε_1) and the imaginary part (ε_2) of dielectric constant can be given by:

$$\varepsilon_1(\lambda) = n^2(\lambda) - k^2(\lambda) \quad (16)$$

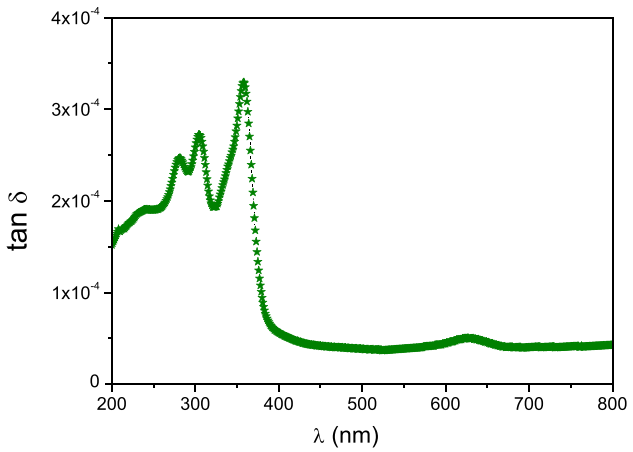

Figure 13. Evolution of the dissipation factor tan δ as a function of the incident photon wavelength for the $(C_8H_{11}BrN)_3BiCl_6$ compound.

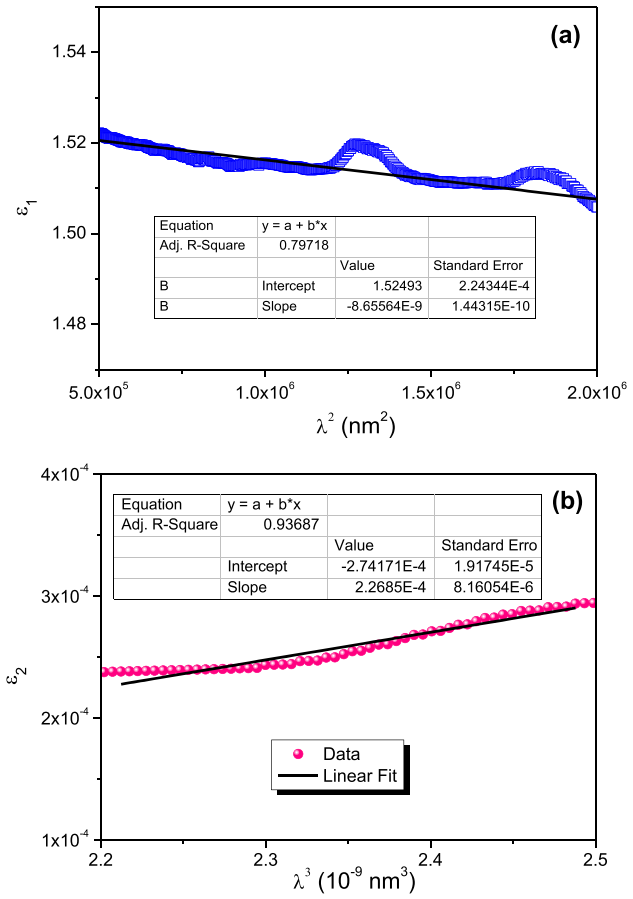

Figure 14. (**a**) Evolution of the real part ε_1 of the dielectric permittivity *vs.* λ^2 and (**b**) the variation of the imaginary part ε_2 *vs.* λ^3.

and

$$\varepsilon_2(\lambda) = 2n(\lambda)k(\lambda). \quad (17)$$

The plots of the real part ε_1 and the imaginary part ε_2 (in the inset) of the dielectric permittivity *vs.* λ for the

$(C_8H_{11}BrN)_3BiCl_6$ compound were illustrated in figure 12. As expected, ε_1 and ε_2 show the same trend as the refractive index due to the smaller values of $k(\lambda)$. On the other hand, the dissipation factor tan δ (or tangent loss) was calculated using the formula [36]:

$$\tan(\delta) = \frac{\varepsilon_2(\lambda)}{\varepsilon_1(\lambda)}. \quad (18)$$

The variation of tan δ against λ, illustrated in figure 13, shows that with increasing the wavelength, the dissipation factor decreases strongly beyond 360 nm. From 400 nm, it becomes almost zero.

In the near infrared domain, the real and the imaginary parts of the dielectric permittivity $\varepsilon^*(\lambda)$ can be expressed by [27]:

$$\varepsilon_1(\lambda) = M_1 - M_2\lambda^2 \quad (19)$$

and

$$\varepsilon_2(\lambda) = M_3\lambda^3. \quad (20)$$

In these relations, M_1, M_2 and M_3 are constants. The evolution of the real part ε_1 of the dielectric permittivity *vs.* λ^2 and the imaginary part ε_2 *vs.* λ^3 are illustrated in figure 14a and b. The obtained values are $M_1 = 1.525$, $M_2 = 8.656\times10^{-9}$ and $M_3 = 2.653\times10^{-13}$ nm^{-3}.

4. Conclusion

The $(C_8H_{11}BrN)_3BiCl_6$ compound was prepared by slow evaporation at room temperature. The optical parameters for this sample were determined on the basis of UV–visible measurements. An analysis of the absorption peaks shows the presence of a particular peak at $\lambda_{des} = 254$ nm located in the UV–C region which has the property of disinfecting water. The optical bandgap was determined by two methods, was evaluated at 3.390 and 3.354 eV, and was confirmed to have a direct behaviour. The allowed direct electronic transitions were at the origin of the photon absorption in the investigated sample. The obtained value of E_g characterizes this compound as a wide bandgap material. The Urbach energy, which characterizes disordered and amorphous materials, shows a low value (128 meV) confirming the good quality of this compound. The evolution of the skin depth δ, the dispersion parameters E_0 and E_d, and optical conductivity σ_{op} with the incident wavelength were studied in detail. In addition, by evaluating the real and imaginary parts of the complex dielectric constant, we have demonstrated that the dissipation factor tan δ has very low values. The refractive index n has important values in the UV region but it falls around unity in the Vis–IR domain. These relevant results show that the $(C_8H_{11}BrN)_3BiCl_6$ compound may be a promoter material for applications in the field of optoelectronic devices.

Acknowledgement

This work was supported by the Tunisian Ministry of Higher Education and Scientific Research.

References

[1] Pietraszko A, Bednarska-Bolek B, Jakubas R and Zielinski P 2001 *J. Phys.: Condens. Matter* **13** 6471
[2] Jakubas R and Sobczyk L 1990 *Phase Trans.* **20** 163
[3] Uchino K 2000 *Ferroelectric devices* (New York: Marcel Dekker)
[4] Zaleski J, Jakubas R, Sobczyk L and Mroz J 1990 *Ferroelectrics* **103** 83
[5] Tu Z and Wu M 2019 *Sci. Bull.* **65** 147
[6] Kulicka B, Jakubas R and Ciunik Z 2004 *J. Phys. Chem. Sol.* **65** 871
[7] Mostafa M F and Hassen A 2006 *Phase Trans.* **80** 302
[8] Zhang S and Lanty G 2009 *J. Acta Mater.* **57** 3301
[9] Ionescu D, Ciobanu B and Radinschi I 2007 *J. Optoelectron. Adv. Mater.* **9** 2608
[10] Kojima A, Teshima K, Shirai Y and Miyasaka T 2009 *J. Am. Chem. Soc.* **131** 6050
[11] Kim H-S, Lee C-R, Im J-H, Lee K-B, Moehl T, Marchioro A *et al* 2012 *J. Sci. Rep.* **2** 591
[12] Mitzi D 1999 in *Progress in inorganic chemistry* K Karlin (ed), vol 48 (New York: John Wiley)
[13] Mitzi D 2001 *J. Chem. Soc. Dalton Trans.* **1** 12
[14] Parola S, Julián-López B, Carlos L D and Sanchez C 2016 *Adv. Funct. Mater.* **26** 6506
[15] Kahouli K, Kahouli A, Khirouni K and Chaabouni S 2020 *J. Mol. Struct.* **1199** 126944
[16] Nagabhushana H, Nagabhushana B M, Kumar M, Premkumar H B, Shivakumara C and Chakradhar R P S 2010 *Phil. Mag.* **26** 3567
[17] Gagandeep S, Kulwant B S L and Sahota H S 2000 *Nucl. Sci. Eng.* **134** 208
[18] Chawla A K, Kaur D and Chandra R 2007 *Opt. Mater.* **29** 995
[19] Lefi R, Ben Naser F and Guermazi H 2017 *J. Alloys Compd.* **696** 1244
[20] Mahfoudh N, Karoui K, Khirouni K and Ben Rhaiem A 2019 *Physica B: Condens. Matter* **554** 126
[21] Mguedla R, Ben Jazia Kharrat A, Saadi M, Khirouni K, Chniba-Boudjada N and Boujelben W 2020 *J. Alloys Compd.* **812** 152130
[22] Marotti R E, Guerra D N, Bello C, Machado G and Dalchiele E A 2004 *Sol. Energy Mater. Sol. Cells* **82** 85
[23] Demichelis F, Minetti-Mezzetti E, Tagliaferro A and Tresso E 1986 *J. Appl. Phys.* **59** 611
[24] Husain S, Keelani A O A and Khan W 2018 *Nano-Structures & Nano-Objects* **15** 17
[25] Shakur H R 2011 *Physica E* **44** 641
[26] Caponetti E, Pedone L, Chillura Martino D, Panto V and Turco Liveri V 2003 *Mater. Sci. Eng. C* **23** 531
[27] Mguedla R, Ben Jazia Kharrat A, Taktak O, Souissi H, Kammoun S, Khirouni K *et al* 2020 *Opt. Mater.* **101** 109742
[28] Ouni B, Boukhachem A, Dabbous S, Amlouk A, Boubaker K and Amlouk M 2010 *Mater. Sci. Semicond. Process.* **13** 281

[29] Wemple S H and Didomenico M 1971 *Phys. Rev. B* **3** 1338
[30] Moss T S 1959 *Optical properties of semiconductors* (London: Butter Worths Scientific Publication LTD)
[31] Sharma P, Dahshan A and Aly K A 2014 *J. Alloys Compd*. **616** 323
[32] Kchaou H, Karoui K, Khirouni K and Ben Rhaiem A 2017 *J. Alloys Compd*. **728** 936
[33] Hassanien A S and Akl Alaa A 2015 *J. Alloys Compd*. **648** 280
[34] Abdel Rafeaa M, Farag A A M and Roushdy N 2009 *J. Alloys Compd*. **485** 660
[35] Omar M A 1987 *Elementary solid physics* (Massachusetts: Addison-Wesley Publishing Company)
[36] Chalana S R, Ganesan V and Mahadevan Pillai V P 2015 *AIP Adv*. **5** 107207